




Higher-order exceptional point in a blue-detuned non-Hermitian cavity optomechanical systemWei Xiong ^{1,*}, Zhuangxia Li,¹ Guo-Qiang Zhang,² Mingfeng Wang,¹ Hai-Chao Li ^{3,†},
Xiao-Qing Luo,^{4,‡} and Jiaojiao Chen ^{5,6,§}¹*Department of Physics, Wenzhou University, Zhejiang 325035, China*²*School of Physics, Hangzhou Normal University, Hangzhou 311121, China*³*College of Physics and Electronic Science, Hubei Normal University, Huangshi 435002, China*⁴*Hunan Province Key Laboratory for Ultra-Fast Micro/Nano Technology and Advanced Laser Manufacture,
School of Electrical Engineering, University of South China, Hengyang 421001, China*⁵*School of Physics and Optoelectronics Engineering, Anhui University, Hefei 230601, China*⁶*Hefei Preschool Education College, Hefei 230013, China*

(Received 17 May 2022; accepted 14 September 2022; published 27 September 2022)

Higher-order exceptional points (EPs) in non-Hermitian systems have attracted great interest due to their advantages in sensitive enhancement and distinct topological features. However, realization of such EPs is still a challenge because more fine-tuning parameters are generically required in quantum systems, compared to the second-order EP (EP2). Here, we propose a non-Hermitian three-mode optomechanical system in the blue-sideband regime for predicting the third-order EP (EP3). By deriving the pseudo-Hermitian condition for the proposed system, one cavity with loss and the other with gain must be required. Then we show that EP3 or EP2 can be observed when the mechanical resonator (MR) is neutral, loss, or gain. For the neutral MR, we find that two degenerate or two nondegenerate EP3s can be predicted by tuning system parameters in the parameter space, while four nondegenerate EP2s can be observed when the system parameters deviate from EP3s, which is distinguished from the previous study in the red-detuned optomechanical system. For the gain (loss) MR, we find that only two degenerate EP3s or EP2s can be predicted by tuning enhanced coupling strength. Our proposal provides a potential way to predict higher-order EPs or multiple EP2s and study multimode quantum squeezing around EPs using blue-detuned non-Hermitian optomechanical systems.

DOI: [10.1103/PhysRevA.106.033518](https://doi.org/10.1103/PhysRevA.106.033518)**I. INTRODUCTION**

Cavity optomechanical (COM) systems, which emerged as a promising platform in quantum information science, have been given considerable attention both theoretically and experimentally [1]. The simplest COM system is made up of a mechanical resonator (MR) nonlinearly coupled to a cavity via radiation pressure, which can be well controlled by strong driving fields. In such mystical systems, abundant effects including sensing [2–5], ground-state cooling [6,7], squeezed light generation [8–10], nonreciprocal transport [11,12], optomechanically induced transparency [13–15], coupling enhancement [16–18], and nonlinear behaviors (e.g., bi- and tristability and chaos) [19,20] have been investigated.

In addition, COM systems have shown huge potential in studying exceptional points (EPs) of non-Hermitian systems [21–27], at which both eigenvalues and eigenvectors coalesce. This is due to the fact that practical COM systems can be characterized by effective non-Hermitian Hamiltonians when decoherence arising from the surrounding environment

is considered. Moreover, the driven COM systems can provide fine-tuning parameters for the requirement of realizing EPs, assisted by strong driving fields. Due to these, EPs have been intensively studied in COM systems, especially for the second-order EPs (EP2s) [22–27] where two eigenvalues and the corresponding eigenvectors coalesce [28–39]. In addition, EP2s are also studied in other systems [40–46]. Around EP2s, many fascinating phenomena such as unidirectional invisibility [47–49], single-mode lasing [50,51], sensitivity enhancement [52,53], energy harvesting [54], protecting the classification of exceptional nodal topologies [55], electromagnetically induced transparency [56–59], and quantum squeezing [60–62] can be studied.

Instead of EP2s, non-Hermitian systems can also host higher-order EPs, where more than two eigenmodes coalesce into one [63–71]. It has been shown that higher-order EPs can exhibit greater advantages than EP2s in spontaneous emission enhancement [68], sensitive detection [72–75], and topological characteristics [76–78]. With these superiorities, higher-order EPs are being intensively studied in various systems [79–88] but attract less attention in non-Hermitian COM systems. For this purpose, there is a need to construct higher-order EPs in non-Hermitian COM systems.

We also note that EPs in non-Hermitian COM systems, including EP2s and EP3s, are mainly focused in the red-sideband regime [21,22]. In this regime, fast oscillating

*xiongweiphys@wzu.edu.cn

†hcl2007@foxmail.com

‡xqluophys@gmail.com

§jjchenphys@hotmail.com

terms related to mode squeezing are neglected. This limits nonclassical quantum effects such as quantum squeezing investigation around EPs. For this, we here theoretically proposed a paradigmatic COM system consisting of a MR coupled to two cavities via radiation pressure for predicting EP3s, where two cavities are, respectively, passive (loss) and active (gain), and driven by two blue-detuned classical fields. First, we derive an effective non-Hermitian Hamiltonian for the proposed COM system and analytically give the pseudo-Hermitian condition of the proposed COM system in the general case. Then, three scenarios are specifically considered in the pseudo-Hermitian condition: (i) the neutral MR, (ii) the passive MR, and (iii) the active MR. In case (i), the proposed non-Hermitian COM system with symmetric coupling strength can host two degenerate EP3s and two nondegenerate EP3s in the parameter space. When we tune the system parameters, deviating from the critical parameters at EP3s, four nondegenerate EP2s can be predicted, which is different from the situation in the red-sideband non-Hermitian COM system. For the cases (ii) and (iii), the proposed non-Hermitian COM system is required to have asymmetric coupling strength for satisfying the pseudo-Hermitian condition. We find that only two degenerate EP3s or two degenerate EP2s can be predicted. By investigating the effects of system parameters on EP3s or EP2s, we find large coupling strength or large frequency detuning is beneficial to observe EPs more clearly. Our proposal provides a promising path to study nonclassical quantum effects around EP2s and EP3s in non-Hermitian COM systems, and it is the first scheme to study higher-order EPs in the blue-detuned COM system, although two-mode quantum squeezing has been investigated in a system with pseudo-antiparity-time symmetry [62].

This paper is organized as follows. In Sec. II, the model is described and the system effective Hamiltonian is given. Then we derive the pseudo-Hermitian condition for the considered non-Hermitian COM system in Sec. III. In Sec. IV, critical parameters of the proposed COM system at EP3 are analytically derived. In Sec. V, phase diagram of the discriminant for the characteristic equation is studied to predict EP3 and EP2. In Sec. VI, EP3 and EP2 in three cases are specifically studied. Finally, a conclusion is given in Sec. VII.

II. MODEL AND HAMILTONIAN

We consider an experimental three-mode optomechanical system [89–91] consisting of two driven cavities (labeled as cavity a and cavity c) coupled to a MR with frequency ω_b via radiation pressure (see Fig. 1). At the rotating frame respect to two laser fields, the Hamiltonian of the total system can be written as (setting $\hbar = 1$) [92]

$$H_{\text{total}} = \delta_a a^\dagger a + \omega_b b^\dagger b + \delta_c c^\dagger c + g_a a^\dagger a (b^\dagger + b) + g_c c^\dagger c (b^\dagger + b) + H_D, \quad (1)$$

where $\delta_{a(c)} = \omega_{a(c)} - \nu_{a(c)}$, with $\omega_{a(c)}$ being the frequency of the cavity a (c), and $\nu_{a(c)}$, is the frequency of the laser field acting on the cavity a (c), is the frequency detuning of the cavity a (c) from the laser field acting on the cavity a (c). g_a and g_c are the single-photon optomechanical coupling strengths of the MR coupled to cavity a and cavity c , respec-

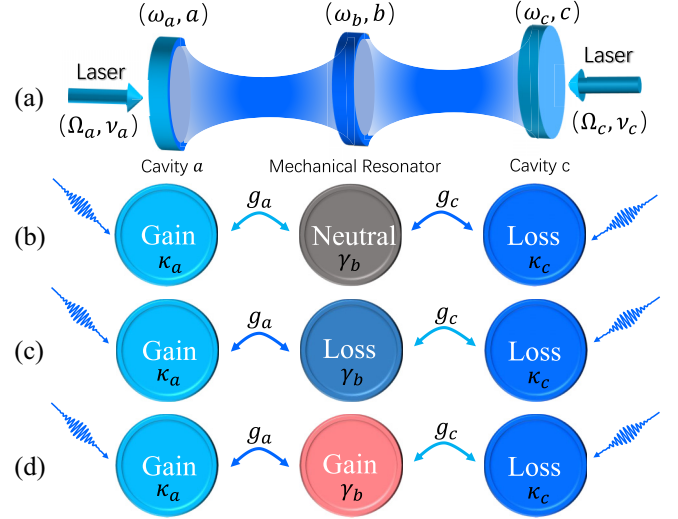


FIG. 1. (a) Schematic diagram of the proposed blue-detuned three-mode optomechanical system. It consists of two cavities labeled as cavity a and cavity c , with respective frequencies ω_a and ω_c , coupled to a common MR with frequency ω_b . The two cavities are driven by two blue-detuned laser fields with frequencies ν_a and ν_b . The corresponding amplitudes are Ω_a and Ω_c . (b) The neutral MR, $\gamma_b = 0$, is considered. (c) The loss MR, i.e., $\gamma_b > 0$, is considered. (d) The gain MR, $\gamma_b < 0$, is considered. In (a), (b), and (c), $\kappa_a (< 0)$ is the gain rate of the cavity a , $\kappa_c (> 0)$ is the loss rate of the cavity, and $g_{a(c)}$ is the single-photon optomechanical coupling strength of the MR coupled to the cavity a (c).

tively. The operators a (c) and a^\dagger (c^\dagger) are the annihilation and creation operators of cavity a (c). The last term $H_D = i(\Omega_a a^\dagger + \Omega_c c^\dagger) + \text{H.c.}$ in Eq. (1) represents the coupling between two cavities and two laser fields with Rabi frequencies Ω_a and Ω_c . As we are interested in the blue-sideband regime of the proposed COM system, $\delta_a, \delta_c < 0$ is assumed below.

In the strong-field limit, the nonlinear COM system can be linearized by writing each operator as the expectation value (a_s, b_s, c_s) plus the corresponding fluctuation $(\delta a, \delta b, \delta c)$. Neglecting the higher-order fluctuations, the linearized Hamiltonian including dissipations can be given by (see details in the Appendix A)

$$H_{\text{eff}} = (\delta'_a - i\kappa_a) \delta a^\dagger \delta a + (\omega_b - i\gamma_b) \delta b^\dagger \delta b + (\delta'_c - i\kappa_c) \delta c^\dagger \delta c + G_a (\delta a^\dagger \delta b^\dagger + \delta a \delta b) + G_c (\delta b^\dagger \delta c^\dagger + \delta b \delta c). \quad (2)$$

Here, fast oscillating terms have been discarded with the condition $|\delta'_{a(c)} + \omega_b| \ll |\delta'_{a(c)} - \omega_b|$ and $|G_{a(c)}| \ll |\delta'_{a(c)}|$, where $\delta'_{a(c)}$ is the effective frequency detuning of the cavity a (c) shifted by the displacement of the mechanical resonator, and $G_{a(c)}$ is the effective optomechanical coupling strength enhanced by the photon number in the cavity a (c). This effective Hamiltonian is the typical three-mode squeezing Hamiltonian without dissipations. For convenience, we assume G_a and G_c to be real, which can be realized by tuning the phase of two laser fields.

III. PSEUDO-HERMITIAN CONDITION

The effective Hamiltonian in Eq. (2) can also be equivalently expressed as

$$H_{\text{eff}} = \begin{pmatrix} \delta'_a - i\kappa_a & G_a & 0 \\ -G_a^* & -\omega_b - i\gamma_b & -G_c^* \\ 0 & G_c & \delta'_c - i\kappa_c \end{pmatrix}, \quad (3)$$

which is just the matrix form of H_{eff} . For the non-Hermitian Hamiltonian in Eq. (3), three eigenvalues can be predicted. When these three eigenvalues are all real, or one is real and the other two are a complex-conjugate pair, the considered three-mode optomechanical system characterized by the Hamiltonian in Eq. (2) or Eq. (3) is pseudo-Hermitian [31,32]. For the pseudo-Hermitian systems, the characteristic polynomial equation

$$|H_{\text{eff}} - \Omega \mathbb{I}| = 0 \quad (4)$$

is the same as

$$|H_{\text{eff}}^* - \Omega \mathbb{I}| = 0, \quad (5)$$

where H_{eff}^* is the complex-conjugate transpose of H_{eff} , \mathbb{I} is a 3×3 identity matrix, and Ω denotes the eigenvalue of the effective Hamiltonian H_{eff} . By expanding Eqs. (4) and (5), and comparing the corresponding coefficients, we can obtain

$$\begin{aligned} \kappa_a + \gamma_b + \kappa_c &= 0, \\ \gamma_b(\delta'_a + \delta'_c) &= \kappa_a(\omega_b - \delta'_c) + \kappa_c(\omega_b - \delta'_a), \\ (\delta'_a\omega_b + \kappa_a\gamma_b)\kappa_c &= G_a^2\kappa_c + G_c^2\kappa_a + (\delta'_a\gamma_b - \kappa_a\omega_b)\delta'_c. \end{aligned} \quad (6)$$

By setting

$$\eta = \kappa_a/\kappa_c, \quad \lambda = G_c/G_a, \quad \Delta_{a(c)} = \delta'_{a(c)} + \omega_b, \quad (7)$$

Eq. (6) can be further simplified as

$$\begin{aligned} \gamma_b + (1 + \eta)\kappa_c &= 0, \\ \Delta_c + \Delta_a\eta &= 0, \\ (1 + \lambda^2\eta)G_a^2 + \eta(1 + \eta)(\Delta_a^2 + \kappa_c^2) &= 0. \end{aligned} \quad (8)$$

Obviously, only when the conditions in Eq. (8) are simultaneously satisfied is the considered three-mode optomechanical system pseudo-Hermitian. From the first condition in Eq. (8), we can see that the decay rates from the cavity a , the mechanical resonator, and the cavity c are required to be balanced. This means a gain effect must be introduced to the considered system. From the third condition, $\eta < 0$ is obtained, which shows that one loss cavity and the other gain cavity are always needed to satisfy the pseudo-Hermitian condition for the proposed COM system in the blue-sideband regime. This situation is completely different from the previous study of EPs using a COM system in the red-sideband regime. Without loss of generality, the cavity a with gain and the cavity c with loss are taken, i.e., $\kappa_a < 0$ and $\kappa_c > 0$. From the third equation in Eqs. (8), it is not difficult to find the fact that $\lambda = 1$ when $\eta = -1$, which indicates that the coupling strengths between the MR and two cavities must be uniform, i.e., $G_a = G_c$. When $\eta \neq -1$,

$$(1 + \eta)(1 + \lambda^2\eta) > 0 \text{ for } \eta \neq -1 \quad (9)$$

is directly given by the third equality in Eqs. (8), which in turn gives rise to a boundary for the parameter λ or equivalently G_a and G_c . Such a boundary can be achieved here due to the tunable parameters Δ_a , Δ_c , G_a , and G_c .

IV. CRITICAL PARAMETERS AT EP3

When the pseudo-Hermitian conditions in Eq. (8) are satisfied and $x = \Omega + \omega_b$ is defined, the characteristic equation in Eqs. (4) reduces to

$$x^3 + c_2x^2 + c_1x + c_0 = 0, \quad (10)$$

where

$$\begin{aligned} c_2 &= (\eta - 1)\Delta_a, \\ c_1 &= (1 + \lambda^2)G_a^2 - \eta\Delta_a^2 + (1 + \eta + \eta^2)\kappa_c^2, \\ c_0 &= (\eta - \lambda^2)G_a^2\Delta_a - (1 + \eta)^2(1 - \eta)\kappa_c^2\Delta_a. \end{aligned} \quad (11)$$

According to Cardano's formula [93], the solutions of this characteristic equation are determined by the discriminant

$$D = B^2 - 4AC, \quad (12)$$

where

$$A = c_2^2 - 3c_1, \quad B = c_1c_2 - 9c_0, \quad C = c_1^2 - 3c_0c_2. \quad (13)$$

For $D < 0$, Eq. (10) has three real roots. But for $D > 0$, Eq. (10) only has one real root and the other two are complex roots. Interestingly, three roots coalesce to the same value Ω_{EP3} at $D = 0$ with $A = B = 0$, which is so-called EP3. For the case of $D = 0$ but $A \neq 0$ and $B \neq 0$, only two roots coalesce to the value Ω_{EP2} , corresponding to EP2.

Below we analytically derive the critical parameters at EP3. When EP3 appears at $\Omega = \Omega_{\text{EP3}}$, we have

$$(\Omega - \Omega_{\text{EP3}})^3 = 0. \quad (14)$$

Comparing coefficients of this equation with Eq. (10),

$$-3x_{\text{EP3}} = c_2, \quad 3x_{\text{EP3}}^2 = c_1, \quad x_{\text{EP3}}^3 = -c_0 \quad (15)$$

are obtained. The first equation directly leads to

$$x_{\text{EP3}} = \frac{1}{3}(1 - \eta)\Delta_a. \quad (16)$$

Substituting this solution back into the second equation in Eqs. (15), the critical coupling strength at EP3 is given by

$$G_{a,\text{EP3}} = 2\kappa_c \left[-\frac{3(1 + \lambda^2)}{1 + \eta + \eta^2} - \frac{1 + \lambda^2\eta}{\eta(1 + \eta)} \right]^{-1/2}, \quad (17)$$

where

$$\Delta_{a,\text{EP3}} = \pm \left[-\frac{1 + \lambda^2\eta}{\eta(1 + \eta)} G_{a,\text{EP3}}^2 - \kappa_c^2 \right]^{1/2} \quad (18)$$

is derived from the third equation in Eqs. (8). As $\Delta_{a,\text{EP3}}^2 \geq 0$, so the minimal value of G_a for predicting EP3 is

$$G_{a,\text{EP3}}^{\text{min}} = \left[-\frac{\eta(1 + \eta)}{1 + \lambda^2\eta} \kappa_c \right]^{1/2}. \quad (19)$$

At EP3, the parameter λ is required to meet

$$\lambda_{\text{EP3}} = \left[\frac{2\eta + 1}{\eta(\eta + 2)} \right]^{3/2}, \quad (20)$$

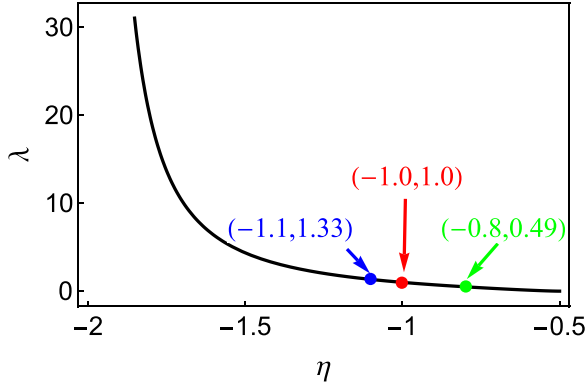


FIG. 2. The parameter λ at EP3 as a function of η . The red, blue, and green dots, respectively, denote $(\eta, \lambda_{\text{EP3}}) = (-1, 1), (-1.1, 1.33), (-0.8, 0.49)$.

which is obtained by substituting the solution in Eq. (16) back into the third equality in Eqs. (15). To see the dependent relationship between λ and η at EP3 more clearly, we plot λ as a function of η in Fig. 2. Obviously, λ monotonously decreases with the absolute value of η . Equation (20) also requires η to satisfy

$$(\eta + 2)(2\eta + 1) < 0. \quad (21)$$

Combining Eqs. (9) and (21), the parameter η for predicting EP3 can take

$$\begin{cases} -2 < \eta < -1, \\ \eta = -1, \\ -1 < \eta < -\frac{1}{2}, \end{cases} \quad (22)$$

leading to

$$\begin{aligned} \gamma_b > 0, & \quad \text{loss mechanical resonator,} \\ \gamma_b = 0, & \quad \text{neural mechanical resonator,} \\ \gamma_b < 0, & \quad \text{gain mechanical resonator.} \end{aligned} \quad (23)$$

The corresponding value of λ_{EP3} is given by Eq. (20).

V. PHASE DIAGRAM FOR PREDICTION OF EP3 AND EP2

Next, we numerically predict EP3 and EP2 via the phase diagram of the discriminant [see Eq. (12)] in the three cases given by Eq. (22).

A. $\eta = -1$

When $\eta = -1$, i.e., $\kappa_a = -\kappa_c$, two optomechanical cavities are gain-loss balanced, and Eq. (8) reduces to

$$\gamma_b = 0, \quad \Delta_c = \Delta_a, \quad \lambda_{\text{EP3}} = 1. \quad (24)$$

For the condition $\gamma_b = 0$, it is difficult to be perfectly satisfied. But for COM systems, the decay rate of the MR is in general much smaller than the decay rate of the optomechanical cavity, i.e., $\gamma_b \ll \kappa_c$. Therefore, we can safely ignore the effect of the decay rate of the MR on EP3, and thus we assume $\gamma_b \approx 0$.

In addition, the coefficients in Eq. (11) are simplified as

$$c_2 = -2\Delta_a, \quad c_1 = 2G_a^2 + \Delta_a^2 + \kappa_c^2, \quad c_0 = -2G_a^2\Delta_a. \quad (25)$$

Correspondingly, the discriminant in Eq. (12) becomes

$$D = \kappa_c^2 \Delta_a^4 - (G_a^4 + 10\kappa_c^2 G_a^2 - 2\kappa_c^4) \Delta_a^2 + (2G_a^2 + \kappa_c^2)^3, \quad (26)$$

and A, B, C in Eq. (13) are

$$\begin{aligned} A &= \Delta_a^2 - 6G_a^2 - 3\kappa_c^2, \\ B &= 2\Delta_a(7G_a^2 - \Delta_a^2 - \kappa_c^2), \\ C &= (2G_a^2 + \Delta_a^2 + \kappa_c^2)^2 - 12G_a^2\Delta_a^2. \end{aligned} \quad (27)$$

In Fig. 3(a), we plot the phase diagram determined by the sign of the discriminant [see Eq. (26)] versus the normalized parameters Δ_a/κ_c and G_a/κ_c , where the purple (yellow) region indicates $D > 0$ ($D < 0$). The boundary curve in red means $D = 0$. The curves in black and green, respectively, denote $A = 0$ and $B = 0$. Obviously, three curves have four cross points, that is, four EP3s in the parameter space can be found according to Cardano's formula [93]. Also, EP2 can be predicted by the red curve only (i.e., $D = 0$, but $A \neq 0$ and $B \neq 0$).

B. $\eta \neq -1$

For the more realistic case, $\eta \neq -1$ is further considered. This indicates that two optomechanical cavities are gain-loss unbalanced. According to Eq. (22), we can discuss the case of $\eta \neq -1$ in two scenarios, i.e., (i) $-2 < \eta < -1$ (or $\gamma_b > 0$); (ii) $-1 < \eta < -\frac{1}{2}$ (or $\gamma_b < 0$). The first scenario indicates that the loss MR and $\lambda > 1$ (i.e., $|G_c| > |G_a|$) are needed to predict EP3 in our proposed COM system. On the contrary, the gain MR and $\lambda < 1$ (i.e., $|G_c| < |G_a|$) is required in the second scenario. As examples, we take $\eta = -1.1$ and $\eta = -0.8$ (see the blue and green dots in Fig. 2). Then we plot the phase diagram of the discriminant with $\eta = -1.1$ [see Fig. 3(b)] and -0.8 [see Fig. 3(c)] versus the normalized parameters G_a/κ_c and G_c/κ_c , where $D = 0$, $A = 0$, and $B = 0$ are shown by the red, black and green curves, respectively. The purple (yellow) region means $D < 0$ ($D > 0$). Obviously, four EP3s (see the red dots) produced by three curves, at which $D = A = B = 0$, can be predicted in both Figs. 3(b) and 3(c) by tuning G_a and G_c . This can be realized because both G_a and G_c are tunable coupling strengths via tuning the Rabi frequencies of the two laser fields. When we deviate G_a (G_b) from $G_{a,\text{EP3}}$ ($G_{b,\text{EP3}}$) at EP3, EP2 emerges [see the red curve only in Figs. 3(b) and 3(c)]. When one parameter is fixed in Figs. 3(a)–3(c), we can easily find that only two EP3s or four EP2s can be observed by varying the other parameter, which is different from the case considered in the red-detuned COM system.

VI. EP3 AND EP2 IN THE BLUE-SIDEBAND THREE-MODE OPTOMECHANICAL SYSTEM

A. $\eta = -1$

In Fig. 3(a), we have predicted that EP3 and EP2 can be observed in our considered system for the case of $\eta = -1$. For clarity, below we study the behavior of three eigenvalues of

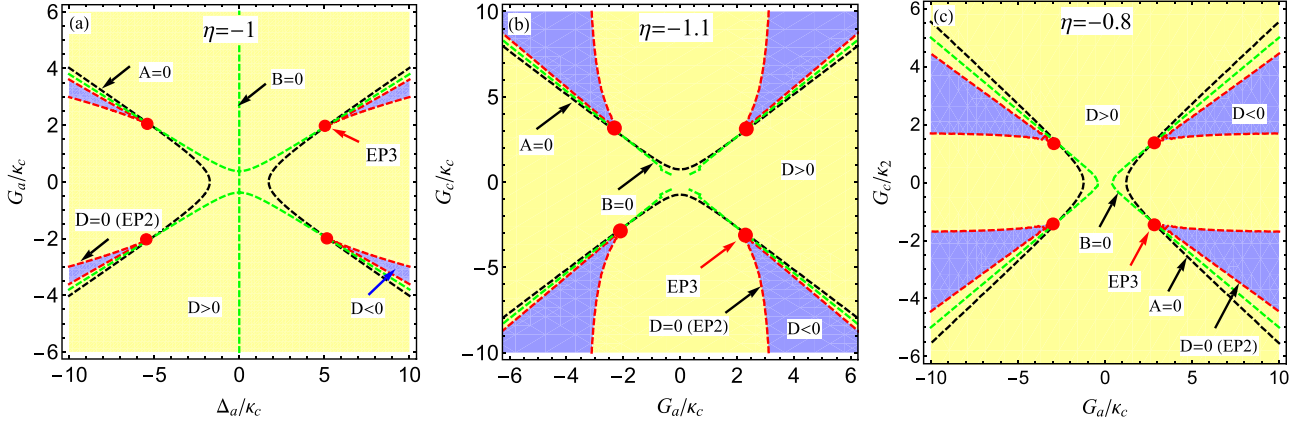


FIG. 3. The phase diagram of the discriminant given by Eq. (12) vs the normalized parameters (a) G_a/κ_c and Δ_a/κ_c ; (b) and (c) G_a/κ_c and G_c/κ_c . In (a), (b), and (c), η is taken as $\eta = -1, -1.1$, and -0.8 , respectively.

the Hamiltonian H_{eff} given by Eq. (2) with different frequency detunings Δ_a and coupling strengths G_a .

In Fig. 4, we plot the real and imaginary parts of the eigenvalue ($x = \Omega + \omega_b$) as a function of the normalized parameter G_a/κ_c with $\Delta_a = 3\sqrt{3}\kappa_c, 10\kappa_c, 15\kappa_c$. For simplicity, we assume that the red, blue, and black curves, respectively, denote three eigenvalues x_1, x_2 , and x_3 for the Hamiltonian H_{eff} hereafter. For $\Delta_a = 3\sqrt{3}\kappa_c$ [see Figs. 4(a) and 4(b)], x_1 is real and the other two eigenvalues (x_2 and x_3) are a complex-conjugate pair in the region of $G_a > G_{a,\text{EP3}}^{(+)} = 2\kappa_c$ or $G_a < G_{a,\text{EP3}}^{(-)} = -2\kappa_c$. But when $G_{a,\text{EP3}}^{(-)} < G_a < G_{a,\text{EP3}}^{(+)}$, x_2 becomes real, and x_1, x_3 become a complex-conjugate pair. At the points $G_a = G_{a,\text{EP3}}^{(\pm)}$ [see the red and black dots in Figs. 4(a) and 4(b)], three eigenvalues coalesce to one value, i.e., $\Omega_{\text{EP3}} = 3.39\kappa_c - \omega_b$, corresponding to two degenerate EP3s. It is not difficult to verify that $D = 0, A = 0$, and $B = 0$ at two EP3s. Then we increase Δ_a to $\Delta_a = 10\kappa_c$ [see Figs. 4(c) and 4(d)]

for deviation from EP3s, that is, $D = 0$ but $A \neq 0$ and $B \neq 0$. For $G_a < G_{a,\text{EP3}}^{(1,-)} = -3.6\kappa_c$ or $G_a > G_{a,\text{EP3}}^{(1,+)} = 3.6\kappa_c$, x_1 is real, and x_2 and x_3 are a complex-conjugate pair. At $G_a = G_{a,\text{EP3}}^{(1,\pm)}$ [see the red and black dots in Figs. 4(c) and 4(d)], x_2 and x_3 coalesce to $\Omega_{\text{EP2}}^{(1)} = 5.22\kappa_c - \omega_b$, corresponding to two degenerate EP2s. By increasing G_a to $G_{a,\text{EP3}}^{(1,-)} < G_a < G_{a,\text{EP3}}^{(1,+)} = -2.99\kappa_c$ or $2.99\kappa_c = G_{a,\text{EP3}}^{(2,+)} < G_a < G_{a,\text{EP3}}^{(2,-)} = 2.99\kappa_c$, the real parts of x_2 and x_3 bifurcate into two values. At $G_a = G_{a,\text{EP3}}^{(2,\pm)}$ [see the blue and green dots in Figs. 4(c) and 4(d)], x_1 and x_3 coalesce to the value $\Omega_{\text{EP2}}^{(2)} = 2.28\kappa_c - \omega_b$, corresponding to two degenerate EP2s. When $G_{a,\text{EP3}}^{(2,-)} < G_a < G_{a,\text{EP3}}^{(2,+)}$, x_2 is real and the other two eigenvalues x_1 and x_3 are complex conjugates. We also find that the separation between two arbitrary EP2s can be increased using larger Δ_a such as $\Delta_a = 15\kappa_c$ [see Figs. 4(c)–4(f)], which indicates that larger Δ_a is beneficial to the distinguishably observe in multiple EP2s.

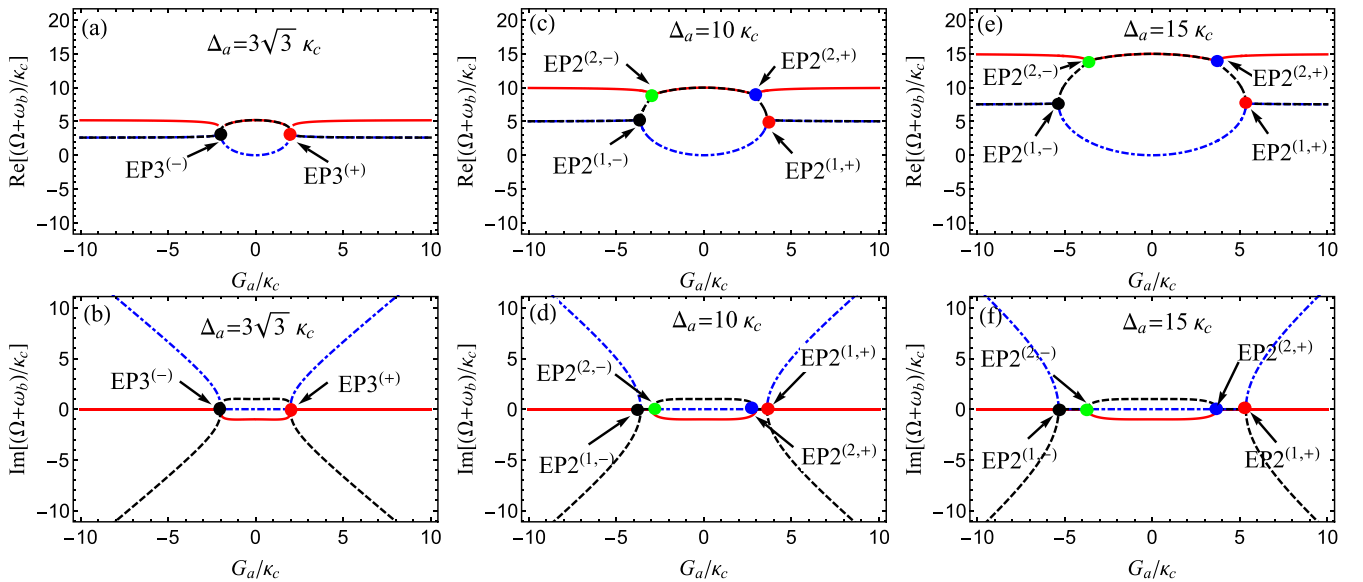


FIG. 4. The real and imaginary parts of the eigenvalue ($x = \Omega + \omega_b$) as a function of the normalized parameter G_a/κ_c with (a) $\Delta_a = 3\sqrt{3}\kappa_c$, (b) $\Delta_a = 10\kappa_c$, and (c) $\Delta_a = 15\kappa_c$. Here $\eta = -1$ and $\lambda = 1$.

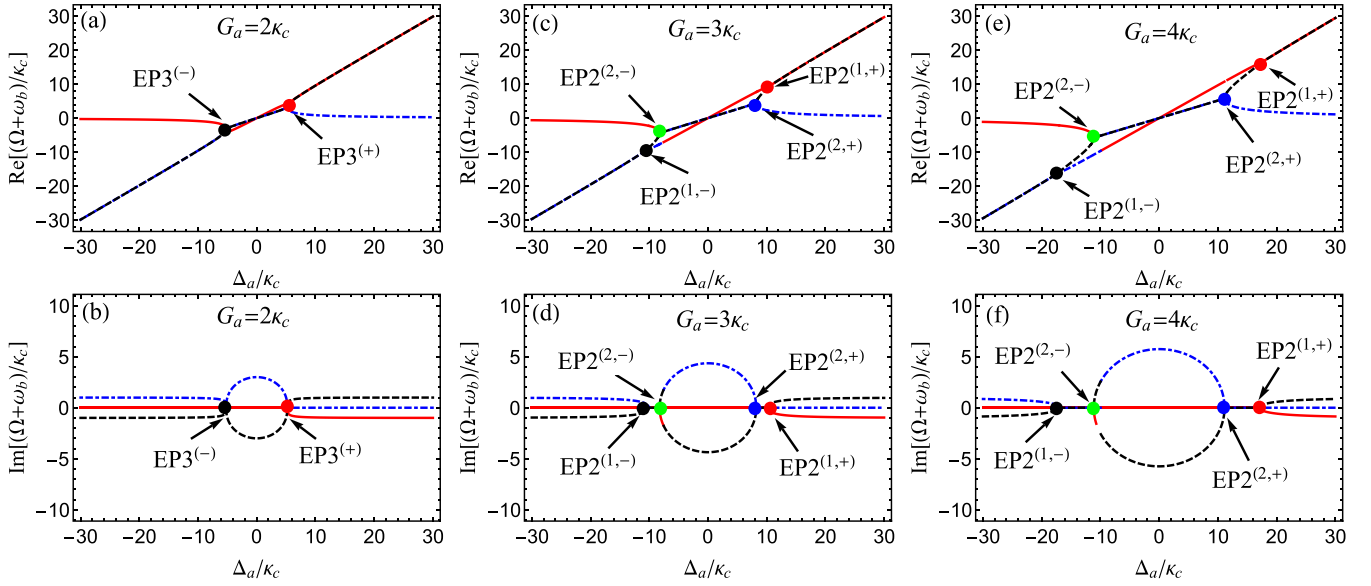


FIG. 5. The real and imaginary parts of the eigenvalue ($x = \Omega + \omega_b$) as a function of the normalized parameter Δ_a/κ_c with (a) $G_a = 2\kappa_c$, (b) $G_a = 3\kappa_c$, and (c) $G_a = 4\kappa_c$. The other parameters are the same as in Fig. 4.

In Fig. 5, we also plot the real and imaginary parts of the eigenvalue ($x = \Omega + \omega_b$) versus the normalized parameter Δ_a/κ_c with different G_a . For $G_a = 2\kappa_c$ [see Figs. 5(a) and 5(b)], x_1 is real, and x_2, x_3 are a complex-conjugate pair when $\Delta_a < \Delta_{a,EP3}^{(-)} = -5.2\kappa_c$. At $\Delta_a = \Delta_{a,EP3}^{(-)} = -5.2\kappa_c$ [see the black dot in Figs. 5(a) and 5(b)], three eigenvalues coalesce to $\Omega_{EP3}^{(1)} = 3.55\kappa_c - \omega_b$, corresponding to EP3. When $\Delta_a < \Delta_{a,EP3}^{(+)} = 5.2\kappa_c$, x_2 and x_3 become a complex-conjugate pair again, and x_1 is real. But when $\Delta_a > \Delta_{a,EP3}^{(+)}$, x_2 becomes real, and x_1 and x_3 are a complex-conjugate pair. At $\Delta_a = \Delta_{a,EP3}^{(+)}$, three eigenvalues reemerge into the same value $\Omega_{EP3}^{(2)} \approx 3.55\Omega_{EP3}^{(1)}$. By increasing G_a to $G_a = 3\kappa_c$ [see the red dots in Figs. 5(c) and 5(d)], two EP3s in Figs. 5(a) and 5(b) split into four EP2s. Specifically, x_1 is real, and x_2 and x_3 are a complex-conjugate pair when $G_a < G_{a,EP2}^{(1,-)} = -10.1\kappa_c$. At $G_a = G_{a,EP2}^{(1,-)} = -10.1\kappa_c$ [see the black dots in Figs. 5(c) and 5(d)], x_2 and x_3 coalesce to $\Omega_{EP2}^{(1)} = -2.27\kappa_c - \omega_b$, corresponding to the first EP2. When $G_{a,EP2}^{(1,-)} < G_a < G_{a,EP2}^{(2,-)} = -8.23\kappa_c$, three eigenvalues are all real but have different values. At $G_a = G_{a,EP2}^{(2,-)}$ [see the green dots in Figs. 5(c) and 5(d)], x_1 and x_3 coalesce to $\Omega_{EP2}^{(2)} = -4.4\kappa_c - \omega_b$, corresponding to the second EP2. For $G_{a,EP2}^{(2,-)} < G_a < G_{a,EP2}^{(2,+)} = 8.23\kappa_c$, x_1 is real, and x_2 and x_3 are a complex-conjugate pair. At $G_a = G_{a,EP2}^{(2,+)}$ [see the blue dots in Figs. 5(c) and 5(d)], x_2 and x_3 reemerge into one value $\Omega_{EP2}^{(3)} \approx \Omega_{EP2}^{(2)}$, corresponding to the third EP2. By tuning G_a to $G_a = G_{a,EP2}^{(1,+)} = 10.1\kappa_c$ [see the red dots in Figs. 5(c) and 5(d)], two different real eigenvalues (i.e., x_1 and x_3) in $G_{a,EP2}^{(2,+)} < G_a < G_{a,EP2}^{(1,+)}$ degenerate as $\Omega_{EP2}^{(4)} = 8.93\kappa_c - \omega_b$, corresponding to the fourth EP2. When G_a exceeds $G_{a,EP2}^{(1,+)}$, x_2 becomes real, and x_2 and x_3 are a complex-conjugate pair. By considering a larger G_a such as $G_a = 15\kappa_c$ [see Figs. 5(e) and 5(f)], we find that EP2s can be distinguished more easily. This indicates that larger coupling strength can also be used to observe EP2s

clearly, similar to the role of the above-discussed frequency detuning Δ_a .

B. $\eta \neq -1$

For the case of $\eta \neq -1$, we also have numerically proved that EP3 and EP2 can be predicted in our proposed blue-sideband optomechanical system by, respectively, taking $\eta = -1.1$ and -0.8 as examples in Figs. 3(b) and 3(c). Here we further specifically study EP3 and EP2 by investigating the eigenvalues of H_{eff} with $\eta = -1.1$ and -0.8 .

For $\eta = -1.1$ (or equivalently $\gamma_b > 0$), which leads to $\lambda = \lambda_{EP3} \approx 1.33$ and $G_{a,EP3}^{\text{min}} = 0.04\kappa_c$, we plot the real and imaginary parts of the eigenvalue ($x = \Omega + \omega_b$) versus the normalized parameter G_a/κ_c with different λ in Fig. 6. From Figs. 6(a) and 6(b), in which $\lambda = \lambda_{EP3}$, we can see that the eigenvalue x_3 denoted by the black curve is always real for arbitrary $G_a \notin (-G_{a,EP3}^{\text{min}}, G_{a,EP3}^{\text{min}})$, and the other two eigenvalues (x_1 and x_2) are a complex-conjugate pair except for at points $G_{a,EP3}^{(\pm)} = \pm 1.82\kappa_c$. At these two points, three eigenvalues coalesce into one value $\Omega_{EP3}^{\pm} = 3.7\kappa_c - \omega_b$, corresponding to two EP3s. When we take $\lambda = 1.2\lambda_{EP3}$, slightly deriving from λ_{EP3} at EP3s, the condition for predicting EP3s is broken, thus EP3 disappears. According to Fig. 3(b), EP2 can be observed. In Figs. 6(c) and 6(d), we plot the real and imaginary parts of the eigenvalue ($x = \Omega + \omega_b$) versus the normalized parameter G_a/κ_c with $\lambda = 1.2\lambda_{EP3}$. It is not difficult to find that three eigenvalues are all real when $G_a > G_{a,EP2}^{(+)} = 2.44\kappa_c$ or $G_a < G_{a,EP2}^{(-)} = -2.44\kappa_c$. At $G_a = G_{a,EP2}^{(\pm)}$, x_1 and x_3 coalesce to $\Omega_{EP2}^{\pm} = 9.05\kappa_c - \omega_b$, corresponding to two EP2s. When $G_{a,EP2}^{(-)} < G_a < G_{a,EP2}^{(+)}$, the real parts of x_1 and x_3 are still degenerate, but their imaginary parts bifurcate into two values.

For the case of $\eta = -0.8$ (or equivalently $\gamma_b < 0$), the behaviors of three eigenvalues are similar to the case of $\eta = -1.1$ for predicting EP3s [see Figs. 7(a) and 7(b)] and EP2s [see Figs. 7(c) and 7(d)].

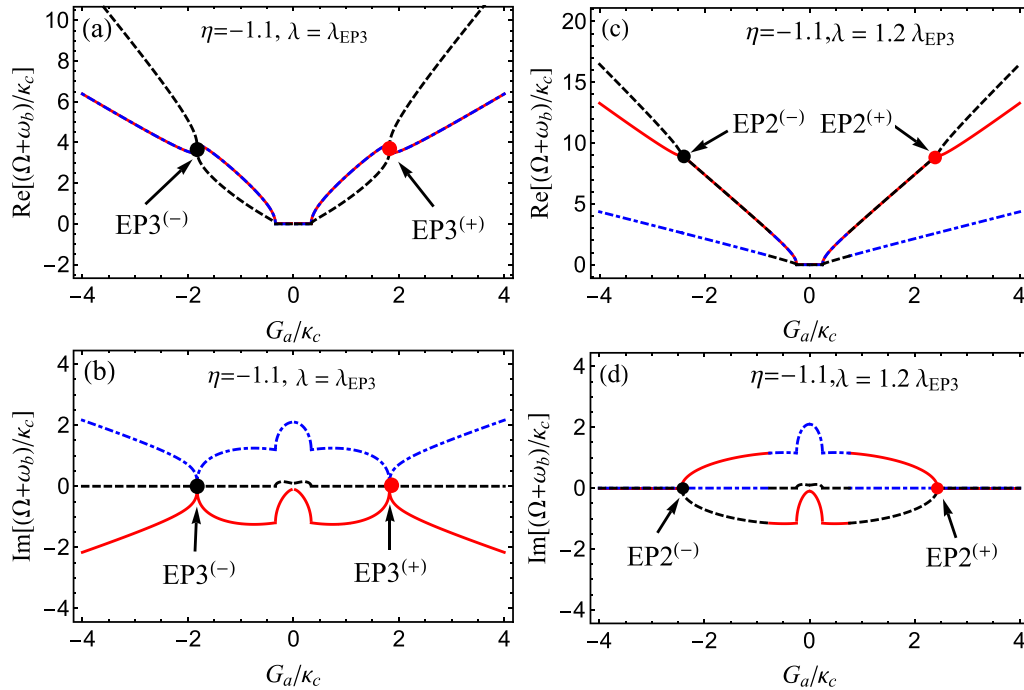


FIG. 6. The real and imaginary parts of the eigenvalue ($x = \Omega + \omega_b$) with $\eta = -1.1$ as a function of the normalized parameter G_a/κ_c with different λ . In (a) and (b), $\lambda = \lambda_{EP3}$. In (c) and (d), $\lambda = 1.2\lambda_{EP3}$.

VII. DISCUSSION AND CONCLUSION

Note that our studies are constrained in the pseudo-Hermitian condition, which can ensure the emergence of EPs in our proposed non-Hermitian COM system. But actually, the strict pseudo-Hermitian condition in general cannot be fully

satisfied, which means that the pseudo-Hermitian condition is broken [see Eq. (6) or Eq. (8)]. For example, the gain and loss in Eq. (6) are not balanced, i.e., $\kappa_a + \kappa_b + \kappa_c \neq 0$. In this situation, we find that both EP3 and EP2 can also be predicted in our setup, as shown in Fig. 8, where $\eta = -1$ and $\kappa_a + \kappa_b + \kappa_c = 0.1\kappa_c$ is taken. This shows that EPs in our

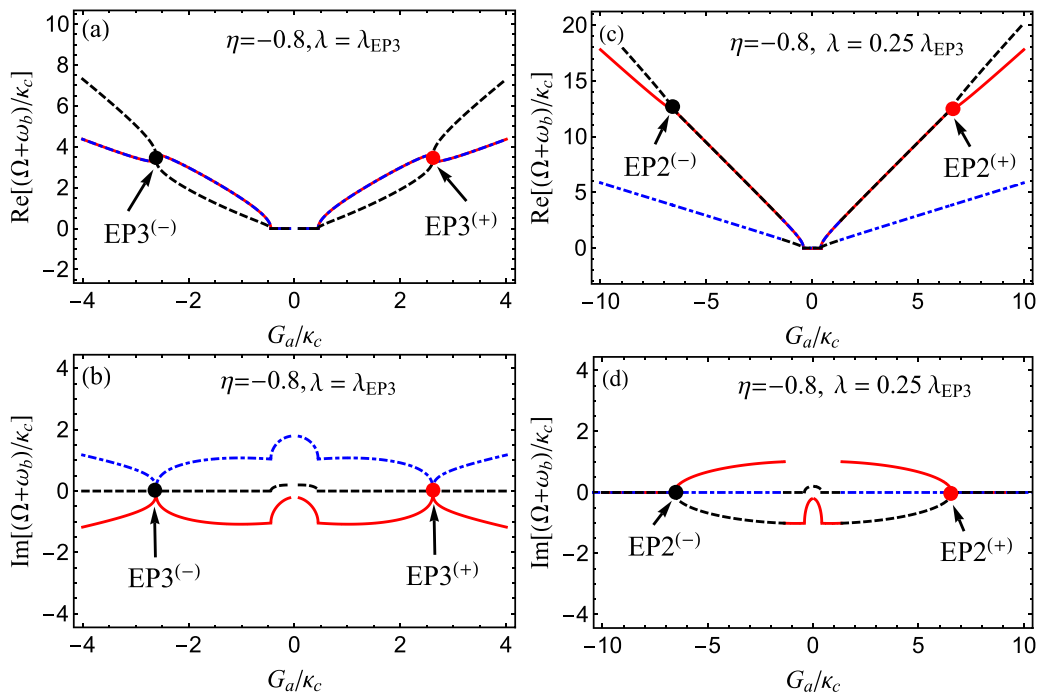


FIG. 7. The real and imaginary parts of the eigenvalue ($x = \Omega + \omega_b$) with $\eta = -0.8$ as a function of the normalized parameter G_a/κ_c with different λ . In (a) and (b), $\lambda = \lambda_{EP3}$. In (c) and (d), $\lambda = 0.25\lambda_{EP3}$.

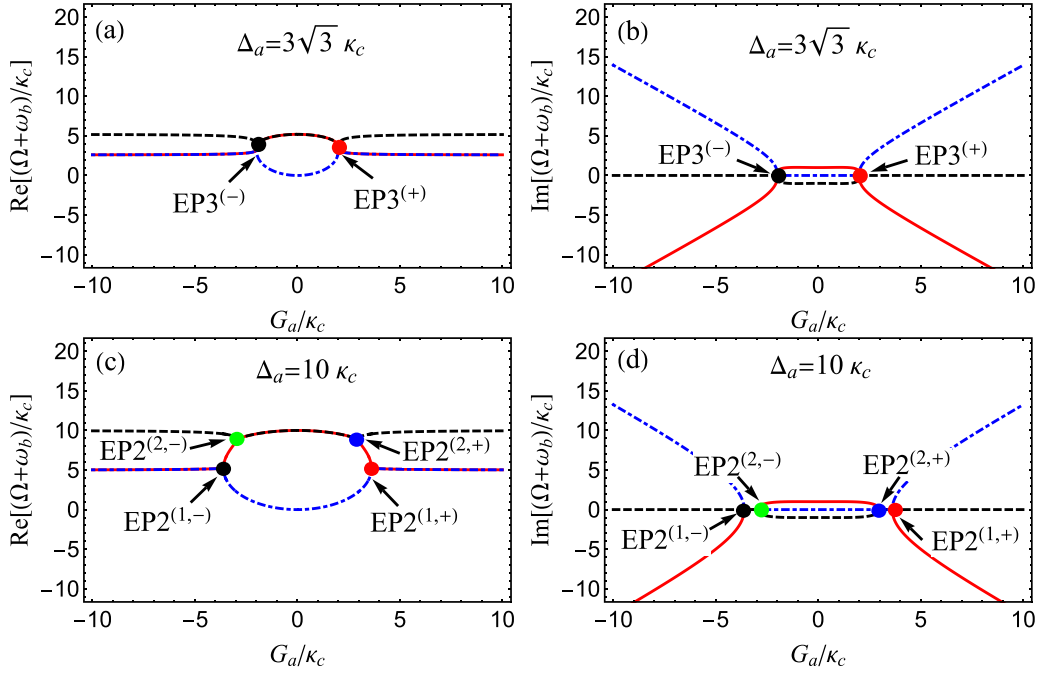


FIG. 8. The real and imaginary parts of the eigenvalue ($x = \Omega + \omega_b$) as a function of the normalized parameter G_a/κ_c with (a) and (b) $\Delta_a = 3\sqrt{3}\kappa_c$, (c) and (d) $\Delta_a = 10\kappa_c$. Here $\eta = -1$, $\lambda = 1$, and $\kappa_a + \kappa_b + \kappa_c = 0.1\kappa_c$.

proposal are robust against the slightly unbalanced gain and loss, which also reveals that the pseudo-Hermitian condition is neither sufficient nor necessary for predicting EPs. For the case of $\eta \neq -1$, we also numerically check it, and the same result is obtained.

In summary, we have proposed a blue-detuned non-Hermitian cavity optomechanical system consisting of a MR coupled to both a passive (loss) and an active (gain) cavity via radiation pressure for predicting EP3s. Under the pseudo-Hermitian condition, the cases of the neutral, loss, and gain MRs are considered. By investigating the phase diagram of the discriminant, we find that two degenerate or two nondegenerate EP3s can be predicted by tuning system parameters in the parameter space for the neutral MR. Also, four nondegenerate EP2s can be observed when system parameters deviate from EP3s, which is distinguished from the previous study in the red-detuned optomechanical system. For the gain (loss) MR, we find that only two degenerate EP3s or EP2s can be predicted by tuning the enhanced coupling strength. By studying the effect of parameters on EP3s or EP2s, we show that large parameters, such as frequency detuning and enhanced optomechanical coupling strength, can be employed to observe EPs more clearly. Our proposal is the first scheme to study higher-order EPs in the blue-detuned COM system, and it provides a potential way to investigate multimode quantum squeezing effects around higher-order EPs

ACKNOWLEDGMENTS

This paper is supported by the key program of the Natural Science Foundation of Anhui (Grant No. KJ2021A1301), the National Natural Science Foundation of China (Grants No. 12205069, No. 11904201 and No. 12104214), and the Natural

Science Foundation of Hunan Province of China (Grant No. 2020JJ5466).

APPENDIX A: THE DERIVATION OF THE EFFECTIVE HAMILTONIAN H_{eff}

In this Appendix, we derive the effective Hamiltonian given by Eq. (2) in the main text. Following the quantum Langevin equation method [94], the dynamics of the proposed system including dissipations can be given by

$$\begin{aligned}\dot{a} &= -(\kappa_a + i\delta_a)a - ig_a a(b^\dagger + b) + \Omega_a + \sqrt{2\kappa_a}a_{\text{in}}, \\ \dot{b} &= -(\gamma_b + i\omega_b)b - ig_a a^\dagger a - ig_c c^\dagger c + \sqrt{2\gamma_b}b_{\text{in}}, \\ \dot{c} &= -(\kappa_c + i\delta_c)c - ig_c c(b^\dagger + b) + \Omega_c + \sqrt{2\kappa_c}c_{\text{in}},\end{aligned}\quad (\text{A1})$$

where $\kappa_{a(c)}$ is the decay rate of the cavity a (c), and γ_b is the decay rate of the MR. Note that when one of the cavities such as the cavity a is subject to the dissipative gain, its corresponding dynamics in Eq. (A1) should be corrected as [95] $\dot{a} = -(i\delta_a - \kappa_a)a - ig_a a(b^\dagger + b) + \Omega_a + \sqrt{2\kappa_a}a_{\text{in}}$, which is different from the first equation in Eqs. (A1). a_{in} , b_{in} , and c_{in} are vacuum input noises with zero expectation value, i.e., $\langle a_{\text{in}} \rangle = \langle b_{\text{in}} \rangle = \langle c_{\text{in}} \rangle = 0$. To linearize the nonlinear equations in Eq. (A1), we write the operators a , b , and c as $a = a_s + \delta a$, $b = b_s + \delta b$, $c = c_s + \delta c$, where $a_s = \varepsilon_a/(\kappa_a + i\Delta_a)$, $b_s = -i(g_a|a_s|^2 + g_c|c_s|^2)/(\kappa_b + i\omega_b)$, $c_s = \varepsilon_c/(\kappa_c + i\Delta_c)$ are steady-state values, and δa , δb , δc are fluctuation operators. Then we substitute these transformations into Eq. (A1). In the strong-field limit, i.e., $|a_s|, |c_s| \gg 1$, higher-order fluctuation terms can be safely neglected. Thus, the dynamics of the fluctuation operators in Eq. (A1) can be

linearized as

$$\begin{aligned}\dot{\delta a} &= -(\kappa_a + i\delta'_a)\delta a - iG_a(\delta b^\dagger + \delta b) + \sqrt{2\kappa_a}a_{\text{in}}, \\ \dot{\delta b} &= -(\gamma_b + i\omega_b)\delta b - i(G_a^*\delta a + G_a\delta a^\dagger) \\ &\quad - i(G_c^*\delta c + G_c\delta c^\dagger) + \sqrt{2\gamma_b}b_{\text{in}}, \\ \dot{\delta c} &= -(\kappa_c + i\delta'_c)\delta c - iG_c(\delta b^\dagger + \delta b) + \sqrt{2\kappa_c}c_{\text{in}},\end{aligned}\quad (\text{A2})$$

where $\delta'_a = \delta_a + g_a a_s(b_s^* + b_s)$ and $\delta'_c = \delta_c + g_c c_s(b_s^* + b_s)$ are the effective frequency detunings of the cavity a and the cavity c , respectively, shifted by the displacement of the MR. In general, such frequency shifts are tiny due to weak single-photon optomechanical coupling strengths. Experimentally, $\delta'_{a(c)} \approx \delta_{a(c)}$ are used. $G_a = g_a a_s$ and $G_c = g_c c_s$ are the effective enhanced optomechanical coupling strengths, which can be tuned by the amplitudes of the two laser fields. Under the condition $|\delta'_{a(c)} + \omega_b| \ll |\delta'_{a(c)} - \omega_b|$ and $|G_{a(c)}| \ll |\delta'_{a(c)}|$, the fast oscillating terms in Eq. (A2) can be neglected. Then Eq. (A2) reduces to

$$\begin{aligned}\dot{\delta a} &= -(\kappa_a + i\delta'_a)\delta a - iG_a\delta b^\dagger + \sqrt{2\kappa_a}a_{\text{in}}, \\ \dot{\delta b} &= -(\gamma_b + i\omega_b)\delta b - iG_a\delta a^\dagger - iG_c\delta c^\dagger + \sqrt{2\gamma_b}b_{\text{in}}, \\ \dot{\delta c} &= -(\kappa_c + i\delta'_c)\delta c - iG_c\delta b^\dagger + \sqrt{2\kappa_c}c_{\text{in}}.\end{aligned}\quad (\text{A3})$$

By rewriting the equations of motion in Eq. (A3) as $\delta a = -i[\delta a, H_{\text{eff}}] + \sqrt{2\kappa_a}a_{\text{in}}$, $\delta b = -i[\delta b, H_{\text{eff}}] + \sqrt{2\gamma_b}b_{\text{in}}$, and $\delta c = -i[\delta c, H_{\text{eff}}] + \sqrt{2\kappa_c}c_{\text{in}}$, the effective non-Hermitian Hamiltonian in the blue-sideband regime can be obtained,

$$\begin{aligned}H_{\text{eff}} &= (\delta'_a - i\kappa_a)\delta a^\dagger \delta a + (\omega_b - i\gamma_b)\delta b^\dagger \delta b + (\delta'_c - i\kappa_c)\delta c^\dagger \delta c \\ &\quad + G_a(\delta a^\dagger \delta b^\dagger + \delta a \delta b) + G_c(\delta b^\dagger \delta c^\dagger + \delta b \delta c),\end{aligned}\quad (\text{A4})$$

which is just the effective Hamiltonian in Eq. (2).

APPENDIX B: STABILITY

From Eq. (A3), we can obtain the following equations:

$$\begin{aligned}\dot{\delta a} &= -(\kappa_a + i\delta'_a)\delta a - iG_a\delta b^\dagger + \sqrt{2\kappa_a}a_{\text{in}}, \\ \dot{\delta b} &= -(\gamma_b + i\omega_b)\delta b - iG_a\delta a^\dagger - iG_c\delta c^\dagger + \sqrt{2\gamma_b}b_{\text{in}}, \\ \dot{\delta c} &= -(\kappa_c + i\delta'_c)\delta c - iG_c\delta b^\dagger + \sqrt{2\kappa_c}c_{\text{in}}, \\ \dot{\delta a}^\dagger &= -(\kappa_a - i\delta'_a)\delta a^\dagger + iG_a\delta b + \sqrt{2\kappa_a}a_{\text{in}}^\dagger, \\ \dot{\delta b}^\dagger &= -(\gamma_b - i\omega_b)\delta b^\dagger + iG_a\delta a + iG_c\delta c + \sqrt{2\gamma_b}b_{\text{in}}^\dagger, \\ \dot{\delta c}^\dagger &= -(\kappa_c - i\delta'_c)\delta c^\dagger + iG_c\delta b + \sqrt{2\kappa_c}c_{\text{in}}^\dagger.\end{aligned}\quad (\text{B1})$$

By setting

$$\begin{aligned}\delta X_a &= \frac{a + a^\dagger}{\sqrt{2}}, \quad \delta Y_a = \frac{a - a^\dagger}{i\sqrt{2}}, \\ \delta X_b &= \frac{b + b^\dagger}{\sqrt{2}}, \quad \delta Y_b = \frac{b - b^\dagger}{i\sqrt{2}}, \\ \delta X_c &= \frac{c + c^\dagger}{\sqrt{2}}, \quad \delta Y_c = \frac{c - c^\dagger}{i\sqrt{2}}, \\ \delta X_{a_{\text{in}}} &= \frac{a_{\text{in}} + a_{\text{in}}^\dagger}{\sqrt{2}}, \quad \delta Y_{a_{\text{in}}} = \frac{a_{\text{in}} - a_{\text{in}}^\dagger}{i\sqrt{2}}, \\ \delta X_{b_{\text{in}}} &= \frac{b_{\text{in}} + b_{\text{in}}^\dagger}{\sqrt{2}}, \quad \delta Y_{b_{\text{in}}} = \frac{b_{\text{in}} - b_{\text{in}}^\dagger}{i\sqrt{2}}, \\ \delta X_{c_{\text{in}}} &= \frac{c_{\text{in}} + c_{\text{in}}^\dagger}{\sqrt{2}}, \quad \delta Y_{c_{\text{in}}} = \frac{c_{\text{in}} - c_{\text{in}}^\dagger}{i\sqrt{2}},\end{aligned}\quad (\text{B2})$$

Eq. (B1) can be rewritten as

$$\dot{u} = Mu + f_{\text{in}},\quad (\text{B3})$$

where $u = [\delta X_a, \delta Y_a, \delta X_b, \delta Y_b, \delta X_c, \delta Y_c]^T$, $f_{\text{in}} = [\delta X_{a_{\text{in}}}, \delta Y_{a_{\text{in}}}, \delta X_{b_{\text{in}}}, \delta Y_{b_{\text{in}}}, \delta X_{c_{\text{in}}}, \delta Y_{c_{\text{in}}}]^T$, and M is given by

$$M = \begin{pmatrix} -\kappa_a & \delta'_a & 0 & -G_a & 0 & 0 \\ -\delta'_a & -\kappa_a & -G_a & 0 & 0 & 0 \\ 0 & -G_a & -\kappa_b & \omega_b & 0 & -G_c \\ -G_a & 0 & -\omega_b & -\kappa_b & -G_c & 0 \\ 0 & 0 & 0 & -G_c & -\kappa_c & \delta'_c \\ 0 & 0 & -G_c & 0 & -\delta'_c & -\kappa_c \end{pmatrix}.\quad (\text{B4})$$

The considered COM system is stable only when the real parts of the eigenvalues λ of the matrix M are all negative, which can be judged by the Routh-Hurwitz criterion [96]. To use this criterion, we expand the characteristic equation $|M - I\lambda| = 0$ as $\lambda^6 + c_5\lambda^5 + c_4\lambda^4 + c_3\lambda^3 + c_2\lambda^2 + c_1\lambda + c_0 = 0$, where the coefficients c_j with $j = 0, 1, \dots, 5$ can be derived using straightforward but tedious algebra. Interestingly, we find $c_5 = 0$ when $\kappa_a + \gamma_b + \kappa_c = 0$, which breaks the Routh-Hurwitz criterion for prediction of the stability. This indicates that when the pseudo-Hermitian condition is strictly satisfied, the considered system is possibly unstable. To ensure that the system is stable, $\kappa_a + \gamma_b + \kappa_c > 0$ is required in experiment. This requirement can be achieved when two cavities are gain-loss balanced and the loss mechanical resonator is employed. Although the pseudo-Hermitian condition is broken, EP3s or EP2s can also be predicted (see Fig. 8). Other stable conditions obtained from the Routh-Hurwitz criterion can be well satisfied. This is due to the tunable frequency detunings and linearized optomechanical coupling strengths via tuning driving fields.

- [1] M. Aspelmeyer, T. J. Kippenberg, and F. Marquardt, Cavity optomechanics, *Rev. Mod. Phys.* **86**, 1391 (2014).
 [2] S. Schreppler, N. Spethmann, N. Brahms, T. Botter, M. Barrios, and D. M. Stamper-Kurn, Optically measuring force near the standard quantum limit, *Science* **344**, 1486 (2014).

- [3] M. Wu, N. L. Y. Wu, T. Firdous, F. F. Sani, J. E. Losby, M. R. Freeman, and P. E. Barclay, Nanocavity optomechanical torque magnetometry and radiofrequency susceptometry, *Nat. Nanotechnol.* **12**, 127 (2017).

- [4] E. Gil-Santos, J. J. Ruz, O. Malvar, I. Favero, A. Lemáître, P. M. Kosaka, S. García-López, M. Calleja, and J. Tamayo, Optomechanical detection of vibration modes of a single bacterium, *Nat. Nanotechnol.* **15**, 469 (2020).
- [5] R. Fischer, D. P. McNally, C. Reetz, G. G. T. Assumpção, T. Knief, Y. Lin, and C. A. Regal, Spin detection with a micromechanical trampoline: Towards magnetic resonance microscopy harnessing cavity optomechanics, *New J. Phys.* **21**, 043049 (2019).
- [6] J. Chan, T. P. M. Alegre, A. H. Safavi-Naeini, J. T. Hill, A. Krause, S. Gröblacher, M. Aspelmeyer, and O. Painter, Laser cooling of a nanomechanical oscillator into its quantum ground state, *Nature (London)* **478**, 89 (2011).
- [7] J. D. Teufel, T. Donner, D. Li, J. W. Harlow, M. S. Allman, K. Cicak, A. J. Sirois, J. D. Whittaker, K. W. Lehnert, and R. W. Simmonds, Sideband cooling of micromechanical motion to the quantum ground state, *Nature (London)* **475**, 359 (2011).
- [8] T. P. Purdy, P. L. Yu, R. W. Peterson, N. S. Kampel, and C. A. Regal, Strong Optomechanical Squeezing of Light, *Phys. Rev. X* **3**, 031012 (2013).
- [9] A. H. Safavi-Naeini, S. Gröblacher, J. T. Hill, J. Chan, M. Aspelmeyer, and O. Painter, Squeezed light from a silicon micromechanical resonator, *Nature (London)* **500**, 185 (2013).
- [10] N. Aggarwal, T. J. Cullen, J. Cripe, G. D. Cole, R. Lanza, A. Libson, D. Follman, P. Heu, T. Corbitt, and N. Mavalvala, Room-temperature optomechanical squeezing, *Nat. Phys.* **16**, 784 (2020).
- [11] H. Xu, L. Jiang, A. A. Clerk, and J. G. E. Harris, Nonreciprocal control and cooling of phonon modes in an optomechanical system, *Nature (London)* **568**, 65 (2019).
- [12] Z. Shen, Y. L. Zhang, Y. Chen, C. L. Zou, Y. F. Xiao, X. B. Zou, F. W. Sun, G. C. Guo, and C. H. Dong, Experimental realization of optomechanically induced non-reciprocity, *Nat. Photon.* **10**, 657 (2016).
- [13] A. Kronwald and F. Marquardt, Optomechanically Induced Transparency in the Nonlinear Quantum Regime, *Phys. Rev. Lett.* **111**, 133601 (2013).
- [14] S. Weis, R. Riviere, S. Deleglise, E. Gavartin, O. Arcizet, A. Schliesser, and T. J. Kippenberg, Optomechanically induced transparency, *Science* **330**, 1520 (2010).
- [15] Y. Liu, M. Davanço, V. Aksyuk, and K. Srinivasan, Electromagnetically Induced Transparency and Wideband Wavelength Conversion in Silicon Nitride Microdisk Optomechanical Resonators, *Phys. Rev. Lett.* **110**, 223603 (2013).
- [16] W. Xiong, J. Chen, B. Fang, M. Wang, L. Ye, and J. Q. You, Strong tunable spin-spin interaction in a weakly coupled nitrogen vacancy spin-cavity electromechanical system, *Phys. Rev. B* **103**, 174106 (2021).
- [17] X. Y. Lü, W. M. Zhang, S. Ashhab, Y. Wu, and F. Nori, Quantum-criticality-induced strong Kerr nonlinearities in optomechanical systems, *Sci. Rep.* **3**, 2943 (2013).
- [18] J. Chen, Z. Li, X. Q. Luo, W. Xiong, M. Wang, and H. C. Li, Strong single-photon optomechanical coupling in a hybrid quantum system, *Opt. Express* **29**, 32639 (2021).
- [19] W. Xiong, D. Y. Jin, Y. Qiu, C. H. Lam, and J. Q. You, Cross-Kerr effect on an optomechanical system, *Phys. Rev. A* **93**, 023844 (2016).
- [20] X. Y. Lü, H. Jing, J. Y. Ma, and Y. Wu, \mathcal{PT} -Symmetry Breaking Chaos in Optomechanics, *Phys. Rev. Lett.* **114**, 253601 (2015).
- [21] W. Xiong, Z. Li, Y. Song, J. Chen, G. Q. Zhang, and M. Wang, Higher-order exceptional point in a pseudo-Hermitian cavity optomechanical system, *Phys. Rev. A* **104**, 063508 (2021).
- [22] H. Jing, Ş. K. Özdemir, X.-Y. Lü, J. Zhang, L. Yang, and F. Nori, \mathcal{PT} -Symmetric Phonon Laser, *Phys. Rev. Lett.* **113**, 053604 (2014).
- [23] Y. L. Liu, R. Wu, J. Zhang, Ş. K. Özdemir, L. Yang, F. Nori, and Y. X. Liu, Controllable optical response by modifying the gain and loss of a mechanical resonator and cavity mode in an optomechanical system, *Phys. Rev. A* **95**, 013843 (2017).
- [24] H. Xu, D. Mason, L. Jiang, and J. G. E. Harris, Topological energy transfer in an optomechanical system with exceptional points, *Nature (London)* **537**, 80 (2016).
- [25] J.-Q. Zhang, J.-X. Liu, H.-L. Zhang, Z.-R. Gong, S. Zhang, L.-L. Yan, S.-L. Su, H. Jing, and M. Feng, Topological optomechanical amplifier in synthetic \mathcal{PT} -symmetry, *Nanophotonics* **11**, 1149 (2022).
- [26] H. Xu, D.-G. Lai, Y.-B. Qian, B.-P. Hou, A. Miranowicz, and F. Nori, Optomechanical dynamics in the \mathcal{PT} - and broken- \mathcal{PT} -symmetric regimes, *Phys. Rev. A* **104**, 053518 (2021).
- [27] X. W. Xu, Y. X. Liu, C. P. Sun, and Y. Li, Mechanical \mathcal{PT} -symmetry in coupled optomechanical systems, *Phys. Rev. A* **92**, 013852 (2015).
- [28] F. Minganti, A. Miranowicz, R. W. Chhajlany, and F. Nori, Quantum exceptional points of non-Hermitian Hamiltonians and Liouvillians: The effects of quantum jumps, *Phys. Rev. A* **100**, 062131 (2019).
- [29] G. Q. Zhang, Z. Chen, D. Xu, N. Shammah, M. Liao, T. F. Li, L. Tong, S. Y. Zhu, F. Nori, and J. Q. You, Exceptional point and cross-relaxation effect in a hybrid quantum system, *PRX Quantum* **2**, 020307 (2021).
- [30] Ş. K. Özdemir, S. Rotter, F. Nori, and L. Yang, Parity-time symmetry and exceptional points in photonics, *Nat. Mater.* **18**, 783 (2019).
- [31] A. Mostafazadeh, Pseudo-Hermiticity versus \mathcal{PT} -symmetry: The necessary condition for the reality of the spectrum of a non-Hermitian Hamiltonian, *J. Math. Phys.* **43**, 205 (2002).
- [32] A. Mostafazadeh, Pseudo-Hermiticity versus \mathcal{PT} -symmetry II: A complete characterization of non-Hermitian Hamiltonians with a real spectrum, *J. Math. Phys.* **43**, 2814 (2002).
- [33] V. V. Konotop, J. Yang, and D. A. Zezyulin, Nonlinear waves in \mathcal{PT} -symmetric systems, *Rev. Mod. Phys.* **88**, 035002 (2016).
- [34] C. M. Bender, B. K. Berntson, D. Parker, and E. Samuel, Observation of \mathcal{PT} phase transition in a simple mechanical system, *Am. J. Phys.* **81**, 173 (2013).
- [35] M. Parto, Y. G. N. Liu, B. Bahari, M. Khajavikhan, and D. N. Christodoulides, Non-Hermitian and topological photonics: Optics at an exceptional point, *Nanophotonics* **10**, 403 (2021).
- [36] E. J. Bergholtz, J. C. Budich, and F. K. Kunst, Exceptional topology of non-Hermitian systems, *Rev. Mod. Phys.* **93**, 015005 (2021).
- [37] J. Wiersig, Review of exceptional point-based sensors, *Photon. Res.* **8**, 1457 (2020).
- [38] L. Feng, R. El-Ganainy, and L. Ge, Non-Hermitian photonics based on parity-time symmetry, *Nat. Photon.* **11**, 752 (2017).
- [39] R. El-Ganainy, K. G. Makris, M. Khajavikhan, Z. H. Musslimani, and D. N. Christodoulides, Non-Hermitian physics and \mathcal{PT} symmetry, *Nat. Phys.* **14**, 11 (2018).

- [40] J. Doppler, A. A. Mailybaev, J. Böhm, U. Kuhl, A. Girschik, F. Libisch, T. J. Milburn, P. Rabl, N. Moiseyev, and S. Rotter, Dynamically encircling an exceptional point for asymmetric mode switching, *Nature (London)* **537**, 76 (2016).
- [41] D. Zhang, X. Q. Luo, Y. P. Wang, T. F. Li, and J. Q. You, Observation of the exceptional point in cavity magnon-polaritons, *Nat. Commun.* **8**, 1368 (2017).
- [42] M. Harder, L. Bai, P. Hyde, and C. M. Hu, Topological properties of a coupled spin-photon system induced by damping, *Phys. Rev. B* **95**, 214411 (2017).
- [43] F. Quijandria, U. Naether, Ş. K. Özdemir, F. Nori, and D. Zueco, \mathcal{PT} -symmetric circuit QED, *Phys. Rev. A* **97**, 053846 (2018).
- [44] G. Q. Zhang, Y. P. Wang, and J. Q. You, Dispersive readout of a weakly coupled qubit via the parity-time-symmetric phase transition, *Phys. Rev. A* **99**, 052341 (2019).
- [45] M. Naghiloo, M. Abbasi, Y. N. Joglekar, and K. W. Murch, Quantum state tomography across the exceptional point in a single dissipative qubit, *Nat. Phys.* **15**, 1232 (2019).
- [46] G. Q. Zhang, Z. Chen, W. Xiong, C. H. Lam, and J. Q. You, Parity-symmetry-breaking quantum phase transition via parametric drive in a cavity magnonic system, *Phys. Rev. B* **104**, 064423 (2021).
- [47] L. Chang, X. Jiang, S. Hua, C. Yang, J. Wen, L. Jiang, G. Li, G. Wang, and M. Xiao, Parity-time symmetry and variable optical isolation in active-passive-coupled microresonators, *Nat. Photon.* **8**, 524 (2014).
- [48] B. Peng, Ş. K. Özdemir, F. Lei, F. Monifi, M. Gianfreda, G. L. Long, S. Fan, F. Nori, C. M. Bender, and L. Yang, Parity-time symmetric whispering-gallery microcavities, *Nat. Phys.* **10**, 394 (2014).
- [49] Z. Lin, H. Ramezani, T. Eichelkraut, T. Kottos, H. Cao, and D. N. Christodoulides, Unidirectional Invisibility Induced by \mathcal{PT} Symmetric Periodic Structures, *Phys. Rev. Lett.* **106**, 213901 (2011).
- [50] L. Feng, Z. J. Wong, R.-M. Ma, Y. Wang, and X. Zhang, Single mode laser by parity-time symmetry breaking, *Science* **346**, 972 (2014).
- [51] H. Hodaei, M.-A. Miri, M. Heinrich, D. N. Christodoulides, and M. Khajavikhan, Parity-time-symmetric microring lasers, *Science* **346**, 975 (2014).
- [52] W. Chen, Ş. K. Özdemir, G. Zhao, J. Wiersig, and L. Yang, Exceptional points enhance sensing in an optical microcavity, *Nature (London)* **548**, 192 (2017).
- [53] M. P. Hokmabadi, A. Schumer, D. N. Christodoulides, and M. Khajavikhan, Non-Hermitian ring laser gyroscopes with enhanced Sagnac sensitivity, *Nature (London)* **576**, 70 (2019).
- [54] L. J. Fernández-Alcázar, R. Kononchuk, and T. Kottos, Enhanced energy harvesting near exceptional points in systems with (pseudo-) \mathcal{PT} symmetry, *Commun. Phys.* **4**, 79 (2021).
- [55] M. Stålhammar, and E. J. Bergholtz, Classification of exceptional nodal topologies protected by \mathcal{PT} symmetry, *Phys. Rev. B* **104**, L201104 (2021).
- [56] A. Guo, G. J. Salamo, D. Duchesne, R. Morandotti, M. Volatier-Ravat, V. Aimez, G. A. Siviloglou, and D. N. Christodoulides, Observation of \mathcal{PT} Symmetry Breaking in Complex Optical Potentials, *Phys. Rev. Lett.* **103**, 093902 (2009).
- [57] C. Wang, X. Jiang, G. Zhao, M. Zhang, C. W. Hsu, B. Peng, A. D. Stone, L. Jiang, and L. Yang, Electromagnetically induced transparency at a chiral exceptional point, *Nat. Phys.* **16**, 334 (2020).
- [58] B. Wang, Z. X. Liu, C. Kong, H. Xiong, and Y. Wu, Mechanical exceptional-point-induced transparency and slow light, *Opt. Express* **27**, 8069 (2019).
- [59] T. X. Lu, H. Zhang, Q. Zhang, and H. Jing, Exceptional-point-engineered cavity magnomechanics, *Phys. Rev. A* **103**, 063708 (2021).
- [60] J. Peřina Jr., A. Lukš, J. K. Kalaga, W. Leoński, and A. Miranowicz, Nonclassical light at exceptional points of a quantum \mathcal{PT} -symmetric two-mode system, *Phys. Rev. A* **100**, 053820 (2019).
- [61] K. Mukherjee and P. C. Jana, Enhancement of squeezing effects in \mathcal{PT} -symmetric coupled microcavities, *Optik* **194**, 163058 (2019).
- [62] X. W. Luo, C. Zhang, and S. Du, Quantum Squeezing and Sensing with Pseudo-Anti-Parity-Time Symmetry, *Phys. Rev. Lett.* **128**, 173602 (2022).
- [63] E. M. Graefe, U. Günther, H. J. Korsch, and A. E. Niederle, A non-Hermitian \mathcal{PT} symmetric Bose-Hubbard model: Eigenvalue rings from unfolding higher-order exceptional points, *J. Phys. A* **41**, 255206 (2008).
- [64] W. D. Heiss, Chirality of wavefunctions for three coalescing levels, *J. Phys. A* **41**, 244010 (2008).
- [65] G. Demange and E.-M. Graefe, Signatures of three coalescing eigenfunctions, *J. Phys. A* **45**, 025303 (2012).
- [66] W. D. Heiss and G. Wunner, A model of three coupled wave guides and third order exceptional points, *J. Phys. A* **49**, 495303 (2016).
- [67] L. Ge, Parity-time symmetry in a flat-band system, *Phys. Rev. A* **92**, 052103 (2015).
- [68] Z. Lin, A. Pick, M. Lončar, and A. W. Rodriguez, Enhanced Spontaneous Emission at Third-Order Dirac Exceptional Points in Inverse-Designed Photonic Crystals, *Phys. Rev. Lett.* **117**, 107402 (2016).
- [69] H. Jing, Ş. K. Özdemir, H. Lü, and F. Nori, High-order exceptional points in optomechanics, *Sci. Rep.* **7**, 3386 (2017).
- [70] M. A. Quiroz-Juárez, A. Perez-Leija, K. Tschernig, B. M. Rodríguez-Lara, O. S. Magaña-Loaiza, K. Busch, Y. N. Joglekar, and R. de J. León-Montiel, Exceptional points of any order in a single, lossy waveguide beam splitter by photon-number-resolved detection, *Photon. Res.* **7**, 862 (2019).
- [71] Z. Bian, L. Xiao, K. Wang, F. A. Onanga, F. Ruzicka, W. Yi, Y. N. Joglekar, and P. Xue, Quantum information dynamics in a high-dimensional parity-time-symmetric system, *Phys. Rev. A* **102**, 030201(R) (2020).
- [72] H. Hodaei, A. U. Hassan, S. Wittek, H. Garcia-Gracia, R. El-Ganainy, D. N. Christodoulides, and M. Khajavikhan, Enhanced sensitivity at higher-order exceptional points, *Nature (London)* **548**, 187 (2017).
- [73] C. Zeng, K. Zhu, Y. Sun, G. Li, Z. Guo, J. Jiang, Y. Li, H. Jiang, Y. Yang, and H. Chen, Ultra-sensitive passive wireless sensor exploiting high-order exceptional point for weakly coupling detection, *New J. Phys.* **23**, 063008 (2021).
- [74] X. G. Wang, G. H. Guo, and J. Berakdar, Enhanced Sensitivity at Magnetic High-Order Exceptional Points and Topological Energy Transfer in Magnonic Planar Waveguides, *Phys. Rev. Appl.* **15**, 034050 (2021).

- [75] C. Zeng, Y. Sun, G. Li, Y. Li, H. Jiang, Y. Yang, and H. Chen, Enhanced sensitivity at high-order exceptional points in a passive wireless sensing system, *Opt. Express* **27**, 27562 (2019).
- [76] K. Ding, G. Ma, M. Xiao, Z. Q. Zhang, and C. T. Chan, Emergence, Coalescence, and Topological Properties of Multiple Exceptional Points and Their Experimental Realization, *Phys. Rev. X* **6**, 021007 (2016).
- [77] P. Delplace, T. Yoshida, and Y. Hatsugai, Symmetry-Protected Higher-Order Exceptional Points and Their Topological Characterization, *Phys. Rev. Lett.* **127**, 186602 (2021).
- [78] I. Mandal and E. J. Bergholtz, Symmetry and Higher-Order Exceptional Points, *Phys. Rev. Lett.* **127**, 186601 (2021).
- [79] A. Roy, S. Jahani, Q. Guo, A. Dutt, S. Fan, M. A. Miri, and A. Marandi, Nondissipative non-Hermitian dynamics and exceptional points in coupled optical parametric oscillators, *Optica* **8**, 415 (2021).
- [80] Q. Zhong, J. Kou, Ş. K. Özdemir, and R. El-Ganainy, Hierarchical Construction of Higher-Order Exceptional Points, *Phys. Rev. Lett.* **125**, 203602 (2020).
- [81] S. M. Zhang, X. Z. Zhang, L. Jin, and Z. Son, High-order exceptional points in supersymmetric arrays, *Phys. Rev. A* **101**, 033820 (2020).
- [82] L. Pan, S. Chen, and X. Cui, High-order exceptional points in ultracold Bose gases, *Phys. Rev. A* **99**, 011601(R) (2019).
- [83] G. Q. Zhang and J. Q. You, Higher-order exceptional point in a cavity magnonics system, *Phys. Rev. B* **99**, 054404 (2019).
- [84] J. Kullig and J. Wiersig, High-order exceptional points of counterpropagating waves in weakly deformed microdisk cavities, *Phys. Rev. A* **100**, 043837 (2019).
- [85] J. Kullig, C. H. Yi, M. Hentschel, and J. Wiersig, Exceptional points of third-order in a layered optical microdisk cavity, *New J. Phys.* **20**, 083016 (2018).
- [86] J. Schnabel, H. Cartarius, J. Main, G. Wunner, and W. D. Heiss, \mathcal{PT} symmetric waveguide system with evidence of a third-order exceptional point, *Phys. Rev. A* **95**, 053868 (2017).
- [87] M. Y. Nada, M. A. K. Othman, and F. Capolino, Theory of coupled resonator optical waveguides exhibiting high-order exceptional points of degeneracy, *Phys. Rev. B* **96**, 184304 (2017).
- [88] X. Y. Wang, F. F. Wang, and X. Y. Hu, Waveguide-induced coalescence of exceptional points, *Phys. Rev. A* **101**, 053820 (2020).
- [89] C. Dong, V. Fiore, M. C. Kuzyk, and H. Wang, Optomechanical dark mode, *Science* **338**, 1609 (2012).
- [90] J. T. Hill, A. H. Safavi-Naeini, J. Chan, and O. Painter, Coherent optical wavelength conversion via cavity optomechanics, *Nat. Commun.* **3**, 1196 (2012).
- [91] R. Andrews, R. W. Peterson, T. P. Purdy, K. Cicak, R. W. Simmonds, C. A. Regal, and K. W. Lehnert, Bidirectional and efficient conversion between microwave and optical light, *Nat. Phys.* **10**, 321 (2014).
- [92] K. Zhang, F. Bariani, Y. Dong, W. Zhang, and P. Meystre, Proposal for an Optomechanical Microwave Sensor at the Sub-photon Level, *Phys. Rev. Lett.* **114**, 113601 (2015).
- [93] G. A. Korn and T. M. Korn, *Mathematical Handbook for Scientists and Engineers* (McGraw-Hill, New York, 1968).
- [94] R. Benguria and M. Kac, Quantum Langevin Equation, *Phys. Rev. Lett.* **46**, 1 (1981).
- [95] C. W. Gardiner and P. Zoller, *Quantum Noise: A Handbook of Markovian and Non-Markovian Quantum Stochastic Methods with Applications to Quantum Optics* (Springer, Berlin, 2000).
- [96] I. S. Gradshteyn and I. M. Ryzhik, *Table of Integrals, Series and Products* (Academic, Orlando, FL, 1980).